SASEC2015
Third Southern African Solar Energy Conference
11 – 13 May 2015
Kruger National Park, South Africa

EXPERIMENTAL TESTING OF A TUBULAR CAVITY RECEIVER FOR A SMALL-SCALE SOLAR THERMAL BRAYTON CYCLE

Le Roux, W.G.[a]*, Meyer J.P.[a] and Bello-Ochende, T.[b]
[a]Department of Mechanical and Aeronautical Engineering, University of Pretoria, South Africa,
[b]Department of Mechanical Engineering, University of Cape Town, South Africa,
*E-mail: willemleroux@gmail.com

ABSTRACT

The open solar thermal Brayton cycle uses air as working fluid, which makes this cycle very attractive for use in water-scarce countries, such as South Africa. An open-cavity tubular solar receiver may be used in a dish-mounted solar thermal Brayton cycle. This solar receiver has been optimised in recent work using the method of entropy generation minimisation. The performance of the optimised open-cavity tubular receiver can be modeled analytically, but this model should be validated. The purpose of the study was to test the receiver in an experimental setup to validate a heat loss model which considers the errors associated with the collector. A 4.8 m diameter aluminium parabolic dish with 45° rim angle was constructed on a two-axis solar tracking system. An optical error of 5 mrad was measured. The receiver had an aperture area of 0.25 m x 0.25 m and was constructed from 88.9 mm diameter stainless steel 316 tube sections. The solar tracking was done manually to provide a tracking error of less than 1°. A blower was used to blow air through the receiver tube to determine the net heat transfer rate to the air. A high-temperature test was also done wherein the receiver was heated up to steady state to determine the convection heat transfer coefficient. The temperatures on the receiver surface were measured with K-type thermocouples. The maximum temperature reached was around 650 K. It is shown that the insulation arrangement around the receiver tube is important.

NOMENCLATURE

a	[-]	Constant
A	[m^2]	Area
A'	[-]	Area ratio
c_p	[J/kgK]	Constant pressure specific heat
f_c	[m]	Focal length
m	[kg]	Mass of the receiver
$\dot{m}$	[kg/s]	Mass flow rate
h	[W/m^2K]	Convection heat transfer coefficient
k	[W/mK]	Thermal conductivity
$\dot{Q}$	[W]	Heat transfer rate
$\dot{Q}^*$	[W]	Rate of available solar heat at receiver cavity
T	[K]	Temperature
t	[m]	Thickness
V	[m/s]	Velocity
x	[m]	Cartesian axis direction
y	[m]	Cartesian axis direction

Special characters

δ	[-]	Solar tracking error
τ	[m]	Shadow displacement
ζ	[-]	Dish slope
η	[-]	Efficiency
ρ	[kg/m^3]	Density
σ	[W/m2K4]	Stefan Boltzmann constant and the heat-generating
ε	[-]	Emissivity
Θ	[-]	Elevation angle
φ_{rim}	[-]	Dish rim angle

Subscripts

ave	Average
col	Overall for the collector
cond	Conduction
conv	Convection
in	At the inlet
ins	Insulation
net	Net
out	At the outlet
rad	Radiation
rec	Receiver
refl	Reflectivity
s	Surface
solar	Direct normal irradiance from the sun
t	Time

INTRODUCTION

The small-scale dish-mounted open solar thermal Brayton cycle (1 – 20 kW) with recuperator has an advantage in terms of cost and mobility and can offer an off-grid electricity solution to the people of the water-scarce Southern Africa. In this cycle, air is heated in a solar receiver. The air is also the working fluid in the power cycle where a micro-turbine is driven for the generation of electricity. Various micro-turbines from the stationary market are available in South Africa off-the-shelf. The addition of a recuperator in the cycle allows for higher cycle efficiencies and a less complex receiver which operates at lower pressure. A solar receiver is used to capture solar radiation coming from a dish concentrator. Solar receivers can be divided into tubular, volumetric and particle receivers. The tubular receiver has the least complex design. A tubular open-cavity receiver and recuperator were optimised for the dish-mounted small-scale solar thermal Brayton cycle by [1] and [2] using the method of total entropy generation minimisation. The optimum receiver tube diameter of 83.3 mm

for a 4.8 m diameter dish found by [1] and [2] is quite large relative to tube diameters used in typical cavity receiver heat loss models. The operation of a dish-mounted solar thermal Brayton cycle receiver can be studied with computer software and algorithms such as SolTrace, as described by [3]. In this work, an open-cavity tubular solar receiver is tested experimentally in a solar collector to validate the use of SolTrace and the heat loss model presented in [1].

EXPERIMENTAL SETUP

Two-axis solar tracker

A two-axis tracking system was designed and built as discussed by [4] (Fig. 1). The tracking system allowed a collector to rotate in the azimuth axis and to slide along two six meter beams to position itself towards the elevation of the sun. Since most commercially available solar tracking sensors, as well as the self-developed sensor discussed in [4], have a tracking error of 1° – 2°, electronic tracking sensors were not used in the experimental tests as they were not accurate enough according to [1]. The tracking was done manually every minute or two during the experiments, by positioning the collector in such a way that the shadow of the receiver was exactly in the middle of the dish. By doing this, the tracking error was expected to be less than 1° according to Eq. (1) since the receiver shadow was allowed a maximum play of 50 mm off its position at the centre of the dish. Other errors due to receiver positioning and tilting of the dish support beam could not be determined. However, by positioning the collector manually, these errors were also accounted for.

Figure 1 Construction of the two-axis solar tracking system.

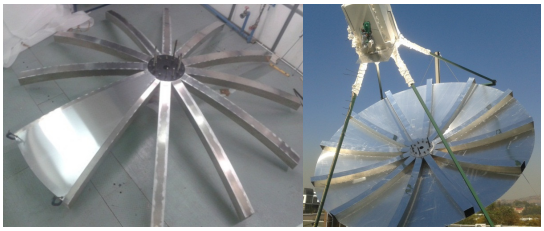

Figure 2 The parabolic solar dish assembled in the laboratory (upside down) and on the two-axis solar tracking system.

$$\delta = \tan^{-1}(\tau/f_c) = \tan^{-1}(0.05/2.897) = \tan^{-1}(0.0173) \approx 1° \quad (1)$$

$$f_c = \sqrt{\frac{(1+\cos\varphi_{rim})^2 \pi R^2}{4\pi \sin^2 \varphi_{rim}}} = \sqrt{\frac{(1+\cos 45)^2 \pi (2.4)^2}{4\pi \sin^2 45}} = 2.897 \text{ m} \quad (2)$$

$$\zeta = \tan^{-1}(dy/dx) = \tan^{-1}(2ax) \quad (3)$$

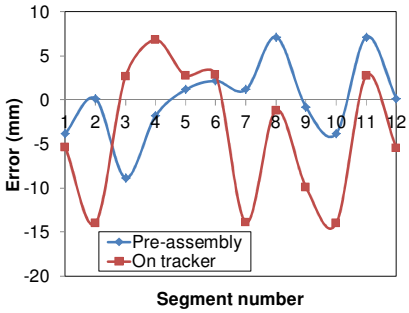

Figure 3 Measured error of the end-height of the twelve dish arms during pre-assembly and on the tracker.

Solar dish

The dish focuses concentrated sun rays onto the receiver. A 4.8 m diameter parabolic dish with rim angle of 45° was designed and built (Fig. 2). The design, manufacturing and installation of the dish created the opportunity to better understand the errors associated with the collector. Polished aluminium alloy arms (Alloy 5754) and low-cost mill-finished aluminium sheets (Alloy 1050 H12/H24 - more than 99.5% Al) were used to construct the dish. The polished aluminium alloy arm sections were laser cut to the correct profile and were then welded to create the twelve tubular arms. The arms were joined together in the middle of the dish with two base plates clamping them from the top and the bottom (Fig. 2). Note that the top reflecting surfaces of the arms had a different parabolic function than the bottom where the sheets were attached so that all the reflective surfaces had the same focus point. The twelve mill-finished pure aluminium sheets with reflectivity of 55% were shaped during installation by riveting them onto the bottom of the positioning arms. The reflectivity was similar to a very dirty polished aluminium dish according to [5].

These sheets were much safer for operation on an experimental setup and were thus chosen to prevent damage to the receiver structure as a result of possible tracking error. These sheets were only used for the purpose of the experiment and for comparison of results with SolTrace, however for commercial purposes, high reflectivity and high specularity reflector sheets should be used. The focal length is calculated with Eq. (2). Also, $f_c = H + R$, thus $H = 0.497$ m and $a = H / R^2 = 0.0863$. The dish arms were assembled in storage and were again assembled on the solar tracker (Fig. 2). Theoretically, the end points of all twelve dish arms should be located at the same height, H, from the bottom base plate. Figure 3 shows the measured error in height of each dish arm as assembled in the laboratory and on the roof. These errors translate into the slope error of the dish which can be calculated with Eq. (3), since the slope of the dish is $y' = 2ax$. For example, a 15 mm error in the height of a dish arm creates a slope error of 10.6 mrad. From Fig. 3, the averaged absolute slope error for the dish due to the arms was calculated as 4.86 mrad. The slope error was assumed to be 5 mrad since the surface finish and roughness on macro scale can also increase the slope error of the dish further.

Solar receiver

The receiver as was discussed in [1] was constructed by welding a number of 90 degree stainless steel (316) elbows and

tubes (Fig. 4) to create the optimum aperture area of 0.25 m x 0.25 m. The receiver tube diameter of 88.9 mm was used for optimum performance in the open solar thermal Brayton cycle with a dish diameter of 4.8 m [1, 2]. The optimum tube diameter was quite large relative to the tubes in typical receiver heat loss models and it was therefore tested to determine any discrepancies. The receiver top could not be manufactured as shown in [1] due to difficult welds. As a result, a ceramic fibre insulation board was used at the top to reflect sun rays back onto the receiver tubes. Also, a gap of 10 mm between each receiver tube coil was required for welding purposes (Fig. 4). Three K-type weld-pad thermocouples were welded onto the receiver surface at the inlet, outlet and in the middle of the receiver (Fig. 4) for temperature measurements. 100 mm thick ceramic fibre insulation board (280 kg/m^3) and insulation blanket, able to withstand temperatures of 1 260 °C, were used to insulate the receiver. The receiver rested on 614 x 614 mm ceramic fibre insulation board with a 0.25 m x 0.25 m aperture. The insulation thermal conductivity was 0.085 W/mK at 200 °C, 0.112 W/mK at 400 °C and 0.145 W/mK at 600 °C according to the manufacturer's specifications. The receiver height from the bottom to the outlet was 765 mm, the width was 427.8 mm and the weight was calculated to be 50 kg.

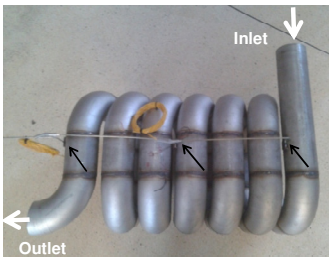

Figure 4 A side view of the solar receiver showing the three weldpad-thermocouples (black arrows) and the flow direction of air (white arrows) from the bottom (inlet) to the top (outlet).

Blower

A 2 500 W leaf blower was attached to the inlet of the receiver and was used to blow air through the receiver tube while it was exposed to the solar heat flux. Six different blower speed settings were used. Measurements were taken with a flow meter at the outlet of the receiver before solar exposure. The averaged mass flow rates created by the blower at the different speed settings were determined. Blower measurements were also done without the receiver attached to determine the increase in air temperature due to the blower. It was found that the increase in air temperature was between 2 °C and 4 °C and was assumed negligible. The elevation of Pretoria is 1 410 m and the average pressure fluctuates around 87 kPa. From this, the air density was calculated to be approximately 1 kg/m^3.

EXPERIMENTAL PROCEDURE

The direct normal irradiance (DNI) and other relevant data were measured with the SOLYS 2 at the University of Pretoria (data available at www.sauran.net). The experiments were conducted during South Africa's winter season which meant the sun's DNI and elevation were at their lowest. The sun's elevation and azimuth angles at the time of the experiments were determined with [6]. The experimental test setup is shown in Fig. 5. A datalogger with accuracy of within 0.5 °C was used and calibration showed that a further error of 1 °C could be expected from the thermocouples. The geometry-dependent effects and temperature-dependent effects on the receiver performance were investigated with Test A and Test B.

Test A

In Test A, the blower was used to blow air through the receiver at six different speed settings while the receiver was exposed to the solar heat flux from the dish. The receiver surface temperatures at the inlet, outlet and in the middle of the receiver tube were measured with the K-type thermocouples and the air temperature at the outlet of the receiver was measured with a T-type thermocouple in the outlet air stream. The purpose of Test A was to determine the optical efficiency of the collector to be used in Test B. Test A was performed to study the geometry-dependant factors contributing to the performance of the receiver.

Test B

For Test B, a high-temperature test was done. The blower and receiver-outlet thermocouple were removed and the inlet and outlet of the receiver were closed off with ceramic fibre insulation blanket. With the receiver at the focus point of the dish, the receiver temperatures were measured until steady-state temperatures were reached. The temperature on the surface of the insulation was also measured on the one side in the middle of the receiver. Thus, the receiver could only lose heat through its aperture with convection and radiation and through the insulation with conduction. This test was done to determine the convection heat loss coefficient on the inside of the cavity and to validate the use of SolTrace and the heat loss models used.

EXPERIMENTAL RESULTS

Test A, Blower test results

Figure 6 shows the measured temperatures of the receiver at the inlet (bottom), middle and outlet (top) surfaces as well as the air temperature at the inlet (air in) and at the outlet (air out) during a test. The measured temperatures at steady state are shown in Table 1 together with the steady-state temperatures of eight other tests performed on different days and with different speed settings. Since the average receiver surface temperature was low, the heat loss rate from the receiver was assumed negligible. The net absorbed heat rates were thus determined with Eq. (4). Figure 7 shows the bottom of the receiver at the focus point of the dish. The receiver tubes are illuminated and the blower is shown behind the heat shield. The blue sky is in the background. From the results it was found that the air temperature at the outlet of the receiver was sometimes lower than the outlet surface temperature and sometimes it was higher. This can be attributed to different flux levels on the inside walls of the cavity at different tracking positions. The efficiency of the collector, η_{col}, was determined from the experiments with Eq. (5) [1] as shown in Table 1. Since $\eta_{rec} \approx 1$, and $\eta_{refl} \approx 0.55$, the optical efficiency could be determined according to Eq. (5) derived from Eq. (6). Note that

the optical efficiency fluctuated between 36% and 54%. These deviations could only be attributed to tracking error which seemed to be a function of the solar elevation and thus a function of the time of day. Note that higher efficiencies were attained when the solar elevation was higher. This can be due to the possible twisting of the structure when lifted upwards (more vertical). The average collector efficiency between 10:00 and 12:00 was found to be 22%, 27% between 12:00 and 13:00 and 22% between 14:00 and 15:00. The absorptance of stainless steel exposed to high tempertures and oxidised can be in the region of 85% and is independent on temperature [7]. Thus it is assumed that the optical results in [1] are also relevant to the experiments performed with minimal error for the receiver initially. From [1], the optical error of the dish for an optical efficiency of between 36% and 54% and for *A'* = 0.0035, was found to be between 20 mrad and 35 mrad. Thus, if the slope error of the dish is 5 mrad, the specularity error of the dish in Eq. (7) is between 17.3 mrad and 33.5 mrad which can be expected from the mill-finished aluminium sheets.

The expected focal spot of the experimental dish on the receiver aperture during the second test on Day 1 was also found with SolTrace for a dish with 5 mrad slope error, 25 mrad specularity error, 1° tracking error, 55% dish reflectivity, DNI of 700 W/m^2 and 85% receiver tube absorbtivity. According to SolTrace, such a collector would have an efficiency of 21%. This efficiency compares well with the efficiency of 23% (Table 1) obtained experimentally during the second test on Day 1. SolTrace showed that a fair amount of the rays would end up around the aperture instead of going into the receiver as also shown in the photo (Fig. 7).

Table 1 Experimental data relevant to Test A.

Day	1	1	2	2	2	3	3	3	3
Blower setting (kg/s)	**0.121**	**0.088**	**0.116**	**0.108**	**0.098**	**0.094**	**0.108**	**0.108**	**0.098**
Start time	12:37	14:36	11:18	12:27	14:26	10:13	11:24	12:25	14:28
Steady state time	13:00	14:56	11:34	12:52	14:40	10:41	12:01	12:45	14:41
Receiver inlet (°C)	39.2	38.8	35.5	38.4	35.9	35.5	-	38.0	36.2
Receiver middle (°C)	45.5	44.9	41.7	45.7	44.4	44.6	-	46.6	45.0
Receiver outlet (°C)	50.4	50.6	46	54.1	50.0	50.1	-	52.2	48.0
Air ambient (°C)	19.8	20.4	17	16.4	18.6	15.9	18.4	19.1	19.9
Air outlet (°C)	52	51	42	49	49	46	50	52	45.0
Collector efficiency (%)	29.5	23.2	19.9	24.9	22.4	21.0	25.3	26.3	21.2
Optical efficiency (%)	53.6	42.2	36.2	45.3	40.7	38.2	46.0	47.8	38.5
Averaged DNI (W/m^2)	780	704	858	821	747	786	783	800	695
Average wind speed (m/s)	0.94	2.27	0.86	1.27	1.54	0.61	0.53	1.1	0.72
Average elevation angle	40.9	36.1	26.8	40.6	37.2	27.6	36.9	40.5	37.2

$$\dot{Q}_{net} = \dot{m} c_p \left(T_{out} - T_{in}\right) \tag{4}$$

$$\eta_{col} = \dot{Q}_{net} / \dot{Q}_{solar} = \eta_{refl} \eta_{rec} \eta_{optical} \tag{5}$$

$$\eta_{rec} = \dot{Q}_{net} / \dot{Q}^{*} = \dot{m} c_{p0} \left(T_{out} - T_{in}\right) / \eta_{optical} \eta_{refl} \dot{Q}_{solar} \tag{6}$$

$$\omega_{optical} = \left(4\omega_{slope}^2 + \omega_{specularity}^2\right)^{1/2} \tag{7}$$

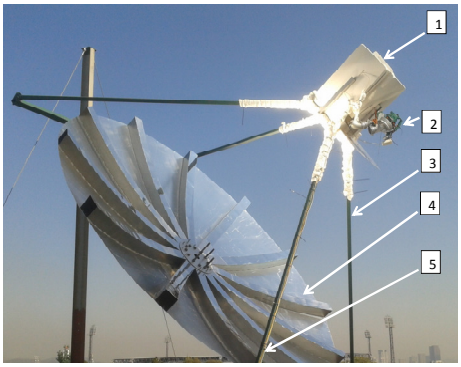

Figure 5 Layout of the experimental setup. 1– Receiver with insulation; 2 – Blower at receiver inlet; 3 – Support structure; 4 – Parabolic dish; 5 – Thermocouple wires to data logger.

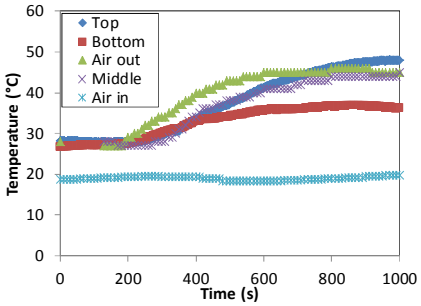

Figure 6 Receiver surface temperature and air temperature measurements at the inlet (bottom) and outlet (top) of the solar receiver with the blower on Speed Setting 3 on Day 3.

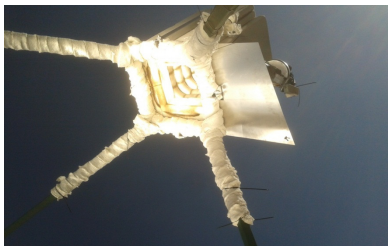

Figure 7 The solar cavity receiver viewed from the bottom.

Test B, High-temperature test results

In this test, the temperature-dependent effects on the receiver performance were investigated. The receiver was heated up to steady state in the collector where after the receiver was placed back to its resting horizontal position. Figure 8 shows the rise in receiver surface temperature at the top (outlet position), bottom (inlet position) and in the middle of the receiver when it was in the focus point of the dish. The temperature rise of the insulation is also shown. The test started at 10:22 and reached steady state after about 167 minutes. The maximum temperature reached at steady state was around 650 K. The

average elevation during the test was 36°. The results show that the top part of the receiver retained its temperature much longer after steady state than the middle and bottom because of hot air being trapped in the cavity. The temperature at the middle and at the bottom of the receiver dropped dramatically as the receiver was tilted horizontally. To validate the heat loss models as described in [1], the average surface temperature of the receiver per second was calculated with Eqs. (8) and (9). According to Test A, the efficiency as calculated with Eq. (10) was 22% between 10:00 and 12:00, and 27% after 12:00.

The convection heat transfer coefficient of the cavity receiver was determined by fitting curves to the experimental results in Fig. 9 and Fig. 10 as calculated with Eq. (8) and Eq. (9) by changing the parameter h_{conv} (the convection heat transfer coefficient) until both curves fit. The only solution where both curves fit, was for $h_{conv} \approx 6.5$ W/m^{2}K and $h_{conv} \approx 1$ W/m^{2}K before and after steady state respectively. Figure 10 shows the conduction heat loss as calculated with the measured average receiver surface temperatures and the calculated average receiver surface temperature. Note that the following constants were used: ε was chosen as 0.7, $k = 0.046$ W/mK [8], $A_{cond} \approx 2$ m^2 and $A_{conv} \approx 1.675$ m^2, as these were the areas exposed to conduction and convection heat loss respectively.

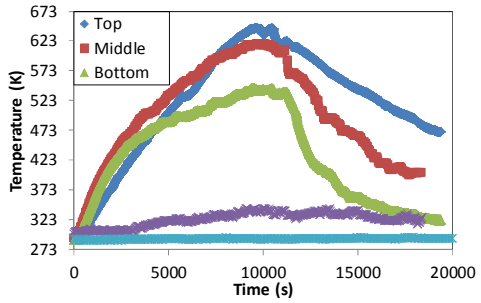

Figure 8 Receiver temperature increase during Test B.

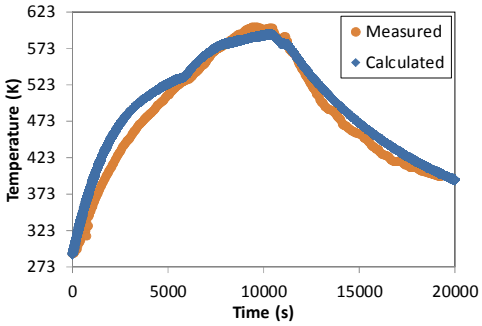

Figure 9 Receiver average surface temperature as a function of time as measured experimentally and as calculated.

$$T_{s,t+1} = \dot{Q}_{net,t} / mc_p + T_{s,t} \tag{8}$$

$$\begin{aligned} \dot{Q}_{net,t} &= \dot{Q}^* - \dot{Q}_{loss,rad,t} - \dot{Q}_{loss,conv,t} - \dot{Q}_{loss,cond,t} \\ &= \dot{Q}^* - \varepsilon\sigma A_{ap}\left(T_{s,t}^{\ 4} - T_0^{\ 4}\right) \\ &\quad - h_{conv} A_{conv}\left(T_{s,t} - T_0\right) - k_{ins} A_{cond}\left(T_{s,t} - T_{ins}\right)/t \end{aligned} \tag{9}$$

$$\dot{Q}^* / \dot{Q}_{solar} = \eta_{optical}\eta_{refl} \tag{10}$$

$$h_{forced} = \left(0.1634 + 0.7498\sin(\theta) - 0.5026\sin(2\theta) + 0.3278\sin(3\theta)\right) \times V^{1.401} = 1.15 \text{ W/m}^2\text{K} \tag{11}$$

$$h_{forced} = 0.1967 \times V^{1.849} = 0.7 \text{ W/m}^2\text{K} \tag{12}$$

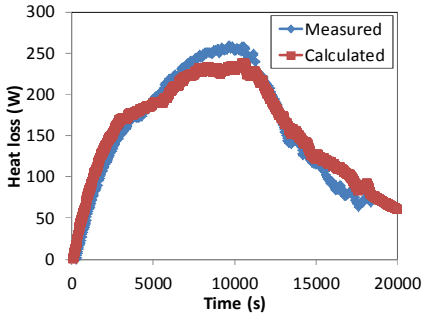

Figure 10 Conduction heat loss from the receiver as calculated with measured experimental data and as calculated.

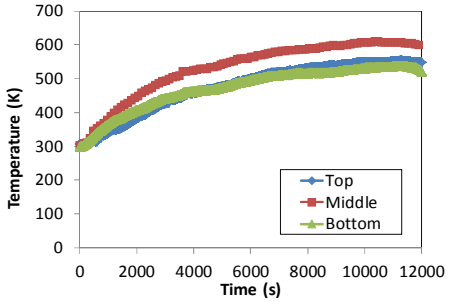

Figure 11 Receiver temperature rise during the second test.

Table 2 Heat loss from the cavity receiver at steady state.

	T_{save} (K)	$\dot{Q}_{loss,cond}$ (W)	$\dot{Q}_{loss,conv}$ (W)	$\dot{Q}_{loss,rad}$ (W)	$\dot{Q}_{loss,total}$ (W)
Test 1	592	236	3 286	287	3 812
Test 2	589	382	1 003	281	1 667

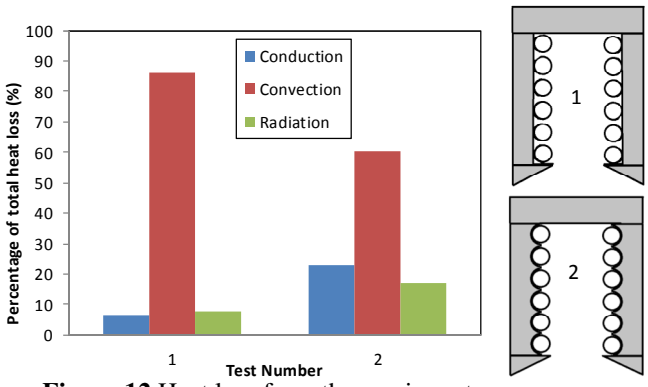

Figure 12 Heat loss from the receiver at an average temperature of 590 K with different insulation arrangements.

The curve-fit result is not very sensitive to the changing of ε or k since convection heat loss dominates in this temperature range. The natural heat transfer coefficient on the inside of the cavity receiver is calculated as 3.7 W/m^{2}K using [9]. This heat transfer coefficient should still be multiplied with a wind factor. The average wind speed during the test was about 2 m/s as was measured with the SOLYS 2. If the wind factor is assumed to

be approximately 1.5 according to [10], the heat transfer coefficient is calculated as 5.55 W/m^{2}K.

According to [11], the forced heat transfer coefficient for the receiver due to a head-on wind of 2 m/s at 36°, which can be added to the natural convection heat transfer coefficient, is calculated in Eq. (11). The forced heat transfer coefficient due to a side wind of 2 m/s, which can be added to the natural convection heat transfer coefficient, is calculated in Eq. (12) [11]. The method given by [11] gives a maximum calculated convection heat transfer coefficient of 4.85 W/m^{2}K. These calculated values of 5.55 W/m^{2}K (using [10]) and 4.85 W/m^{2}K (using [11]) show that the average convection heat transfer coefficient before steady state as determined experimentally (6.5 W/m^{2}K) is about 20% higher.

After inspection of the experimental setup, it was noted that the insulation were not covering the receiver fully and small gaps between the insulation boards were noted. These gaps appeared due to the thermal expansion of the receiver. Also note that convection heat loss was taking place over most of the receiver tube area, since only parts of it was making contact with the insulation. This was as a result of the large diameter tube used and due to the 10 mm gap between the tube coils which had to be present for welding purposes. The test was repeated a second time but this time with insulation blanket stuffed in between all the small gaps between the insulation board and the receiver tube so that air could not flow around the tubes but only on the inside of the cavity. The second test reached more or less the same average receiver surface temperature as in the first test but with a much lower solar input (Fig. 11).

The second test is compared with the first test in Table 2 and Fig. 12. The results show that the insulation arrangement in the second test is much more efficient. Also note that in the second test, the temperature in the middle of the receiver was the higher temperature. This can be attributed to the solar heat flux distribution as shown in [1] as well as a smaller convection heat loss area in the first test. Note that the convection heat loss rate percentage can thus be significantly reduced (Fig. 12) by placing the insulation around the tubes correctly and making sure that there are no gaps between the insulation and the receiver. The convection heat transfer coefficient of the cavity receiver in the second test was determined in a similar way as was done for the first test. It was found that $h_{conv} \approx 4.5$ W/m^{2}K before steady state and $h_{conv} \approx 0.8$ W/m^{2}K after steady state when the receiver was placed in the horizontal position. These results compared much better with the theory and thus it is concluded that the insulation arrangement of the second test is more favourable. Note that for these curve fits, the convection heat loss area was assumed to be half of what it was in the first test due to the different insulation arrangement, thus $A_{cond} \approx 2.4$ m^2 and $A_{conv} \approx 0.838$ m^2.

SUMMARY AND CONCLUSION

An experimental setup consisting of a two-axis solar tracker with a 4.8 m diameter dish and receiver with aperture area of 0.25 m x 0.25 m and tube diameter of 88.9 mm was built and tested to better understand the errors associated with the collector. The geometry-dependent and temperature-dependent factors on the performance of the receiver were investigated. The efficiency of the collector was determined by attaching a blower to the receiver inlet so that the neat absorbed heat rate could be determined. It was found that the optical efficiency of the dish varied between 36% and 54%. Results showed that SolTrace was a valid tool for ray tracing. A high-temperature test on the receiver was also conducted to validate the conduction and convection heat loss models. The receiver was heated up to steady state in two tests with different insulation arrangements. It was shown that for the large tube diameter the arrangement of the insulation was important and that the convection heat loss could be significantly reduced by arranging the insulation correctly around the receiver tube. The convection and conduction heat loss models were verified experimentally to a certain extent, however the heat loss models should still be validated at higher receiver temperatures of around 1 150 K which is typical for the Brayton cycle.

REFERENCES

[1] Le Roux, W.G., Bello-Ochende, T., Meyer, J.P., 2014. The efficiency of an open-cavity solar receiver for a small-scale solar thermal Brayton cycle. Energy Conversion and Management, Vol. 84, pp. 457–470.

[2] Le Roux, W.G., Bello-Ochende, T., Meyer, J.P., 2014. Optimisation of an open rectangular cavity receiver and recuperator used in a small-scale solar thermal Brayton cycle with thermal losses. In: Proceedings of the 10th International Conference on Heat Transfer, Fluid Mechanics and Thermodynamics (HEFAT2014), 14–16 July, Orlando, USA.

[3] Bode, S.J., Gauché, P., 2012. Review of optical software for use in concentrated solar power systems. In: Proceedings of the Southern African Solar Energy Conference (SASEC 2012), May, Stellenbosch, South Africa.

[4] Le Roux, W.G., Mwesigye, A., Bello-Ochende, T., Meyer, J.P., 2014. Tracker and collector for an experimental setup of a small-scale solar thermal Brayton cycle. In: Proceedings of the 2nd Southern African Solar Energy Conference (SASEC 2014), 27-29 January, Port-Elizabeth, South Africa.

[5] Stine, B.S., Harrigan, R.W., 1985. Solar Energy Fundamentals and Design. New York: John Wiley & Sons.

[6] SunEarthTools, 2014. SunEarthTools.com, Tools for consumers and designers of solar. Available at: http://www.sunearthtools.com/dp/tools/pos_sun [2014/07/29].

[7] Valkonen, E., Karlsson, B., 1982. Spectral selectivity of a thermally oxidized stainless steel. Solar Energy Materials, Vol. 7, pp. 43-50.

[8] Tiasa, 2001. Thermal Insulation Handbook. The Thermal Insulation Association of Southern Africa, Association of Architectural Aluminium Manufacturers of South Africa. Available at: www.aaamsa.co.za [2014/08/16].

[9] Harris, J.A., Lenz, T.G., 1983. Thermal performance of solar concentrator/cavity receiver systems. Solar Energy, Vol. 34(2), pp. 135-142.

[10] Prakash, M., 2013. Numerical studies on natural convection heat losses from open cubical cavities. Journal of Engineering, pp. 1-9.

[11] Ma, R.Y., 1993. Wind effects on convective heat loss from a cavity receiver for a parabolic concentrating solar collector. Sandia Laboratory Report SAND92–7293.